X-ray powder diffraction data of $LaNi_{0.5}Ti_{0.45}Co_{0.05}O_3$, $LaNi_{0.45}Co_{0.05}Ti_{0.5}O_3$, and $LaNi_{0.5}Ti_{0.5}O_3$ perovskites

Mariana M. V. M. Souza,[1] Alex Maza,[2] and Pablo V. Tuza [2,a)]

[1]*Escola de Química, Universidade Federal do Rio de Janeiro (UFRJ), Centro de Tecnologia, Bloco E, Sala 206, Rio de Janeiro, RJ CEP 21941-909, Brazil*

[2]*Departamento de Ciencias de la Energía y Mecánica, Carrera de Petroquímica, Universidad de las Fuerzas Armadas – ESPE sede Latacunga, Campus Académico General Guillermo Rodríguez Lara, Belisario Quevedo, Latacunga, Cotopaxi 050150, Ecuador*

(Received 2 March 2020; accepted 14 December 2020)

In the present work, $LaNi_{0.5}Ti_{0.45}Co_{0.05}O_3$, $LaNi_{0.45}Co_{0.05}Ti_{0.5}O_3$, and $LaNi_{0.5}Ti_{0.5}O_3$ perovskites were synthesized by the modified Pechini method. These materials were characterized using X-ray fluorescence, scanning electron microscopy, and powder X-ray diffraction coupled to the Rietveld method. The crystal structure of these materials is orthorhombic, with space group *Pbnm* (No 62). The unit-cell parameters are $a = 5.535(5)$ Å, $b = 5.527(3)$ Å, $c = 7.819(7)$ Å, $V = 239.2(3)$ Å^3, for the $LaNi_{0.5}Ti_{0.45}Co_{0.05}O_3$, $a = 5.538(6)$ Å, $b = 5.528(4)$ Å, $c = 7.825(10)$ Å, $V = 239.5(4)$ Å^3, for the $LaNi_{0.45}Co_{0.05}Ti_{0.5}O_3$, and $a = 5.540(2)$ Å, $b = 5.5334(15)$ Å, $c = 7.834(3)$ Å, $V = 240.2(1)$ Å^3, for the $LaNi_{0.5}Ti_{0.5}O_3$. [doi:10.1017/S0885715620000767]

Key words: perovskite, $LaNi_{0.5}Ti_{0.45}Co_{0.05}O_3$, $LaNi_{0.45}Co_{0.05}Ti_{0.5}O_3$, $LaNi_{0.5}Ti_{0.5}O_3$, X-ray diffraction

I. INTRODUCTION

Perovskites oxides are compounds with the formula ABO_3, where A is a lanthanide or alkali earth metal and B is a transition metal (Mefford *et al.*, 2014). They can be represented by B-cations placed in the center of octahedra connected through the vertices, creating octahedra layers and cavities between them. The octahedra vertices are occupied by oxygen atoms, while A cations are located at the center of the cavities.

Double perovskites (*DPs*), mostly represented by the formula $A'A''B'B''O_6$, where the number of primes indicate distinct possible metal ions with the same amount (Anderson *et al.*, 1993), present various physical and chemical properties (Anderson *et al.*, 1993; Shaheen and Bashir, 2010; Ezzahi *et al.*, 2011). B-cation sublattice types known for *DPs* are rock-salt, layered, and random (Anderson *et al.*, 1993). The rock-salt and layered sublattices characterize ordered *DPs*. Random-like *DPs* can be assumed to be perovskites with equal number of two different B-cations. They have been applied as electrode materials for fuel cells (Deng *et al.*, 2009; Li *et al.*, 2011) or a catalyst for some reactions (Campbell, 1992; Huang *et al.*, 2009; Tuza and Souza, 2016).

Hydrogen is an important raw material for chemical industries and oil refineries. Because of environmental regulations, low quality of crude oil, and China and India's growing markets, the increase of H_2 consumption is expected (Zohuri, 2019). H_2 is mainly produced by steam reforming of methane (Iulianelli *et al.*, 2016), which has been carried out over various catalysts, including perovskites. For instance, Ni^0/La_2O_3, a catalyst obtained from $LaNiO_3$ perovskite, showed the catalytic activity for steam reforming of methane. However, catalyst deactivation was observed due to coking. For instance, Provendier *et al.* (2001) prepared an $LaNiO_3$ perovskite catalyst for steam reforming of methane. The authors observed catalyst deactivation and coke formation over the catalyst surface.

Titanium inclusion in $LaNiO_3$ perovskite can mitigate coke deposition on Ni^0/La_2O_3. For instance, Hayakawa *et al.* (1997) synthesized $Ni/Ca_{0.8}Sr_{0.2}TiO_3$ as a catalyst for CO_2 reforming of CH_4. Catalyst performance was related to Ni dispersion over the perovskite and strong interaction between nickel and perovskite containing titanium. Urasaki *et al.* (2005) used an $Ni/SrTiO_3$ catalyst for steam reforming of methane. Hindering production of carbon species due to oxygen mobility in perovskite containing titanium was related to high catalytic activity of an $Ni/SrTiO_3$ catalyst.

By substituting Ni^{3+} from $LaNiO_3$ by Ti^{4+} such that equal amount of B-cations is attained, either the random ($LaNi_{0.5}Ti_{0.5}O_3$, orthorhombic symmetry, and space group *Pbnm* (Rodríguez *et al.*, 1999)) or the rock-salt (La_2NiTiO_6, monoclinic symmetry, and space group $P2_1/n$ (Rodríguez *et al.*, 2002; Pérez-Flores *et al.*, 2011; Yang *et al.*, 2012)) sublattice was achieved. Ni^0/La_2TiO_5, which is obtained after reduction of $LaNi_{0.5}Ti_{0.5}O_3$ perovskite, showed both catalytic activity and stability for steam reforming of methane because of the metal–support interaction (Tuza and Souza, 2016).

Partial substitution of either NiO_6 or TiO_6 from double perovskite $LaNi_{0.5}Ti_{0.5}O_3$ by CoO_6, i.e., $LaNi_{0.5}Ti_{0.45}Co_{0.05}O_3$ and $LaNi_{0.45}Co_{0.05}Ti_{0.5}O_3$, and the corresponding influence on crystal structure, reductive behavior, and catalytic activity for steam reforming of methane were reported in a previous work (Tuza and Souza, 2017). These properties were completely different for $LaNi_{0.5}Ti_{0.45}Co_{0.05}O_3$ when compared with the other materials, which was attributed to different metal–support

a)Author to whom correspondence should be addressed. Electronic mail: pvtuza@espe.edu.ec

interaction between Ni^0 (for the $LaNi_{0.5}$ $Ti_{0.5}O_3$) or Ni^0–Co^0 (for cobalt-containing perovskites) and the corresponding supports, as confirmed from quantitative phase analysis for these perovskites after reduction with 10% H_2/N_2. It is worth noting that $LaNi_{0.5}Ti_{0.5}O_3$ can be a double perovskite with the random ordering of *B*-cations (Anderson *et al.*, 1993). Moreover, only the catalyst obtained from the perovskite synthesized by partial substitution of Ni^{2+} from $LaNi_{0.5}Ti_{0.5}O_3$ by Co^{2+} in 0.05 mol did not present catalytic stability for the investigated reaction.

In this work, we report powder X-ray diffraction (XRD) data for $LaNi_{0.5}Ti_{0.45}Co_{0.05}O_3$, $LaNi_{0.45}Co_{0.05}Ti_{0.5}O_3$, and $LaNi_{0.5}Ti_{0.5}O_3$ materials, which were published in the Powder Diffraction File™ with the PDF numbers 00-69-0417, 00-69-0418, and 00-69-0419, respectively.

II. MATERIALS AND METHODS

A. Synthesis

$LaNi_{0.5}Ti_{0.45}Co_{0.05}O_3$ and $LaNi_{0.45}Co_{0.05}Ti_{0.5}O_3$ materials were prepared by the modified Pechini method and reported in a previous work (Tuza and Souza, 2016, 2017). Briefly, adequate amounts of precursors (lanthanum nitrate hexahydrate ($La(NiO_3)_3 \cdot 6H_2O$, 99.5%), nickel nitrate hexahydrate ($Ni(NiO_3)_2 \cdot 6H_2O$, 97%), cobalt nitrate hexahydrate ($Co(NiO_3)_2 \cdot 6H_2O$, 100%), and titanium isopropoxide ($C_{12}H_{28}O_4Ti$, 97%) from Sigma-Aldrich) were dissolved in water. Metal citrates were prepared by heating metal solutions to 60 °C, to which citric acid was added. The polyester solution was achieved after adding ethylene glycol at 90 °C to a solution composed of lanthanum, nickel, cobalt, and titanium citrates. The resin obtained by evaporation of the polyester solution was calcined at 240 °C for 1 h and 450 °C for 4 h. The material was milled and then calcined in air at 800 °C for 17 h. Moreover, $LaNi_{0.5}Ti_{0.5}O_3$ perovskite was synthesized by using the same method. The perovskites were obtained in the form of black powders.

B. Characterization

The chemical composition of the as-prepared materials was determined by X-ray fluorescence analysis, which was

TABLE I. Chemical composition determined from X-ray fluorescence, Sycos, X-ray density, atomic coordinates, unit-cell parameters, bond lengths, bonding angles, and conventional discrepancy factors from Rietveld refinement of powder XRD data for $LaNi_{0.5}Ti_{0.45}Co_{0.05}O_3$, $LaNi_{0.45}Co_{0.05}Ti_{0.5}O_3$, and $LaNi_{0.5}Ti_{0.5}O_3$.

	$LaNi_{0.5}Ti_{0.45}Co_{0.05}O_3$[a]	$LaNi_{0.45}Co_{0.05}Ti_{0.5}O_3$[b]	$LaNi_{0.5}Ti_{0.5}O_3$[c]	$LaNi_{0.5}Ti_{0.5}O_3$ (ICSD: 88851)[d]
La (wt%)	71.3	70.9	71.1	
Ni (wt%)	16.6	15.2	16.5	
Ti (wt%)	10.3	12	12.4	
Co (wt%)	1.8	1.9		
Sycos (°)	0.04590	−0.01622	−0.00685	
X-ray density (g cm^{-3})	6.685	6.661	6.643	6.631
Average crystallite size (nm)	35.8	32.7	27.1	
a (Å)	5.535(5)	5.538(6)	5.540(2)	5.517
b (Å)	5.527(3)	5.528(4)	5.5334(15)	5.555
c (Å)	7.819(7)	7.825(10)	7.834(3)	7.856
V (Å^3)	239.2(3)	239.5(4)	240.2(1)	240.59
La: *x*	−0.0072(9)	−0.0053(12)	−0.0046(4)	−0.0048
y	0.0226(7)	0.0184(8)	0.0198(3)	0.0206
z	0.25	0.25	0.25	0.25
Ni: *x y z*	0.5 0 0	0.5 0 0	0.5 0 0	0.5 0 0
Ti: *x y z*	0.5 0 0	0.5 0 0	0.5 0 0	0.5 0 0
Co: *x y z*	0.5 0 0	0.5 0 0	–	
O1: *x*	0.275(8)	0.251(11)	0.253(3)	0.281
y	0.278(8)	0.284(7)	0.292(2)	0.249
z	0.048(3)	0.041(3)	0.0443(12)	0.036
O2: *x*	0.02	0.02	0.02	0.02
y	0.489(5)	0.496(6)	0.478(2)	0.499
z	0.25	0.25	0.25	0.25
B–O1[e]	2.01(4) × 2	2.11(5) 2	2.146(14) × 2	2.10348 × 2
	1.99(4) × 2	1.86(5) 2	1.847(14) × 2	1.85749 × 2
B–O2[f]	1.9588(19) × 2	1.960(3) × 2	1.9654(10) × 2	1.967 × 2
B–O1–*B*[g]	155(2)	160(2)	157.4(6)	162.1
B–O2–*B*[h]	172.6(2)	173.4(3)	170.4(1)	173.6
*R*p/*R*wp (%)	20.5/26.8	21.4/26.8	12.7/14.6	
*R*bragg (%)	6.406	6.224	4.31	
$\chi 2$	1.15	1.18	1.68	

Theoretical chemical composition of La (wt%)/Ni (wt%)/Ti (wt%)/Co (wt%).
[a]72.07%/15.22%/11.18%/1.53%.
[b]72.27%/13.74%/12.45%/1.54%.
[c]72.28%/15.27%/12.45%/0.
[d]Reference: ICSD (2017).
[e]Bond lengths (Å), in which *B* is equal to Ni/Ti or Ni/Ti/Co, according to *B*-cations.
[f]Bond lengths (Å), in which *B* is equal to Ni/Ti or Ni/Ti/Co, according to *B*-cations.
[g]Bonding angles (°), in which *B* is equal to Ni/Ti or Ni/Ti/Co, according to *B*-cations.
[h]Bonding angles (°), in which *B* is equal to Ni/Ti or Ni/Ti/Co, according to *B*-cations

https://doi.org/10.1017/S0885715620000767 Published online by Cambridge University Press

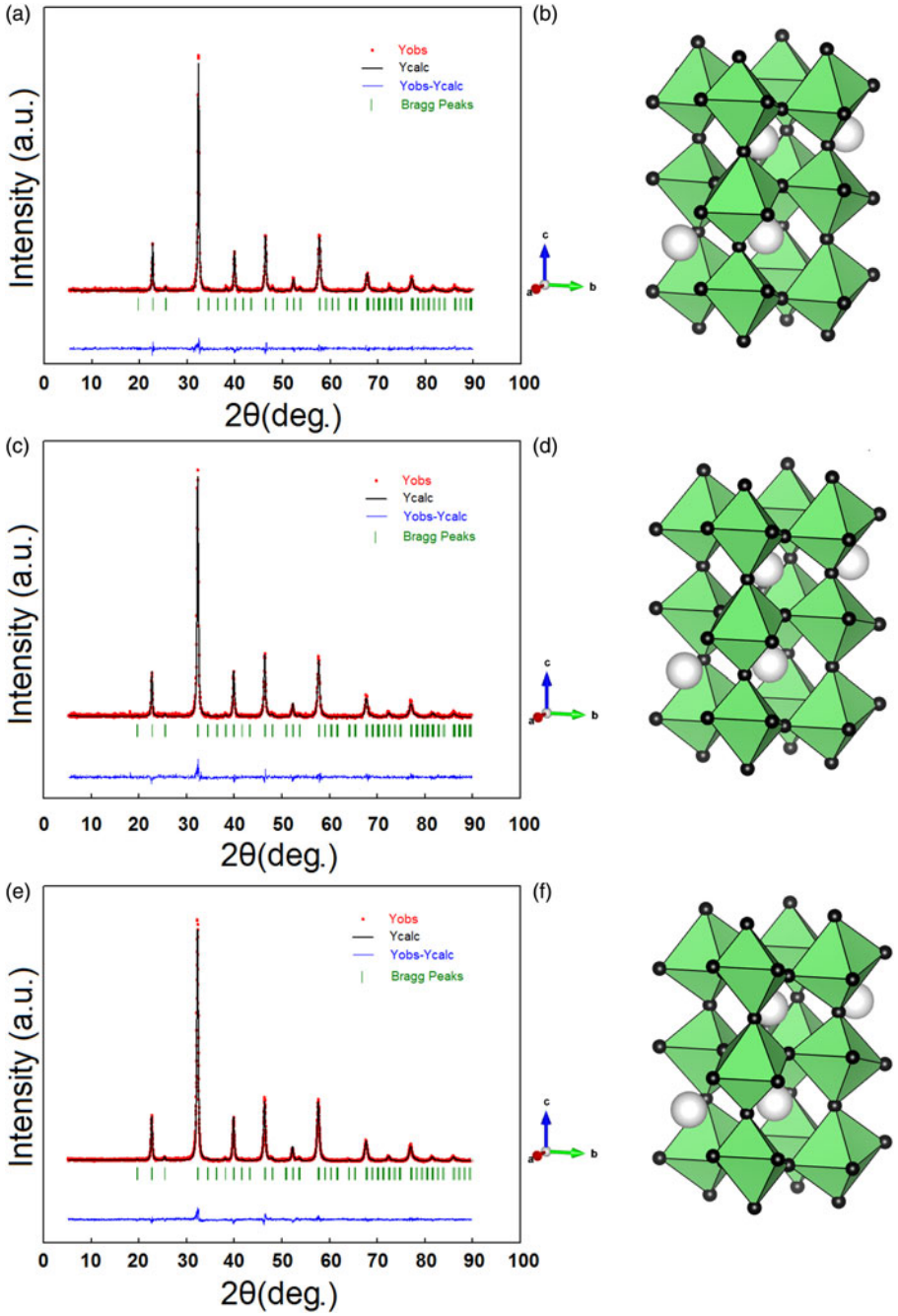

Figure 1. Observed (red symbols), calculated (black line), and difference (blue line) XRD profiles for (a) $LaNi_{0.5}Ti_{0.45}Co_{0.05}O_3$, (c) $LaNi_{0.45}Co_{0.05}Ti_{0.5}O_3$, and (e) $LaNi_{0.5}Ti_{0.5}O_3$. Crystal structure of (b) $LaNi_{0.5}Ti_{0.45}Co_{0.05}O_3$, (d) $LaNi_{0.45}Co_{0.05}Ti_{0.5}O_3$, and (f) $LaNi_{0.5}Ti_{0.5}O_3$.

carried out using a Rigaku Primini Spectrometer equipped with a Pd X-ray tube operating at 50 W (40 kV, 1.25 mA), and a ZSX software package. A sample amount around 200 mg was packed on a polyethylene sample cup, covered with polypropylene thin-film, and then fixed with a ring. Chemical composition was expressed on the weight percentage basis of the cation amount for each sample. Sample images were recorded by means of scanning electron microscopy (Model Quanta™ 450 FEG, FEI Co) operating with an accelerating voltage of 20 kV. Previously, samples were sputter-coated with a gold-based layer for enhancing image quality.

Powder XRD patterns were recorded at room temperature using the Rigaku Miniflex II X-ray diffractometer equipped with a graphite monochromator and Cu$K\alpha$ radiation (30 kV and 15 mA), 2θ range 5–90°, step size and counting time per step equal to 0.02° and 6 s (for $LaNi_{0.5}Ti_{0.5}O_3$ perovskite) or 0.05° and 1 s (for cobalt-containing perovskites). A mass amount approximately equal to 300 mg was packed on a quartz specimen holder as a thin layer of powdered compound. The *d*-values were calculated using Cu$K\alpha$ radiation.

The Rietveld method of powder XRD patterns was performed using the Fullprof Program (Rodríguez-Carvajal, 1993). The structural model of $LaNi_{0.5}Ti_{0.5}O_3$ perovskite (space group *Pbnm*) (ICSD, 2017) was used as a starting point to refine the corresponding structures for the as-synthesized samples. The background (fourth-degree polynomial), the scale factor, the unit-cell parameters, three

https://doi.org/10.1017/S0885715620000767 Published online by Cambridge University Press

TABLE II. Powder diffraction data of $LaNi_{0.5}Ti_{0.45}Co_{0.05}O_3$.

$2\theta_{obs}$ (°)[a]	d_{obs} (Å)	$(I/I_0)_{obs}$	h	k	l	$2\theta_{calc}$ (°)[b]	$2\theta_{calc}$ (°)[c]	d_{calc} (Å)[d]	$\Delta 2\theta$ (°)[e]
22.748	3.906	109.1	0	0	2	22.747	22.727	3.909	0.001
25.455	3.496	32.9	1	1	1	25.447	25.444	3.498	0.009
32.374	2.763	1000	1	1	2	32.379	32.352	2.765	−0.005
38.156	2.357	11.9	1	0	3	38.159	38.134	2.358	−0.003
39.926	2.256	150.3	2	0	2	39.937	39.877	2.259	−0.011
43.231	2.091	1.6	2	1	2	43.236	43.233	2.091	−0.005
46.460	1.953	328.7	2	2	0	46.458	46.396	1.955	0.002
47.898	1.898	19.4	2	2	1	47.912	47.912	1.897	−0.014
50.775	1.797	3.7	1	2	3	50.786	50.863	1.794	−0.011
52.302	1.748	44.9	2	2	2	52.303	52.263	1.749	−0.001
53.735	1.704	31.7	1	3	1	53.698	53.685	1.706	0.037
57.727	1.596	196.9	3	1	2	57.719	57.662	1.597	0.009
67.771	1.382	161	2	2	4	67.783	67.722	1.382	−0.013
72.439	1.304	17.7	3	1	4	72.431	72.423	1.304	0.008
77.105	1.236	84	1	1	6	77.097	77.078	1.236	0.008
81.666	1.178	28.8	4	2	2	81.652	81.533	1.180	0.014
82.776	1.165	9.9	1	3	5	82.798	82.74	1.165	−0.022
86.156	1.128	46.5	4	0	4	86.158	86.004	1.129	−0.002
87.229	1.117	14.4	2	4	3	87.232	87.202	1.117	−0.003
89.495	1.094	0.4	1	0	7	89.493	89.419	1.095	0.002

F(20) = 16.13 (0.0090, 138) (Smith and Snyder, 1979).
[a]Corrected observed peak positions.
[b]Peak positions calculated using the McMaille program.
[c]Peak positions calculated using the Fullprof program.
[d]Interplanar distance calculated using the Fullprof program.
[e]$\Delta 2\theta$ (°) = $^{a}2\theta_{obs}$ (°) − $^{b}2\theta_{calc}$ (°).

halfwidth parameters, La1 at (x, y, 0.25), O1 at (x, y, z), and O2 at (y, 0.25) atomic coordinates, and the sample displacement, Sycos, were refined. Sycos is equal to the ratio between a correction parameter attributed to sample displacement error, in degrees, and cosine of θ angle, where θ is measured in radians (Rodríguez-Carvajal, 2001). Since a satisfactory fit could not be achieved, "x" atomic coordinate for O2 was not refined. The isotropic displacement parameter was maintained at 0.5 $Å^2$, as suggested for atoms in a metal oxide (Attfield *et al.*, 2004). Peak shapes of powder XRD patterns were described using the pseudo-Voigt function. The fraction of site occupancy for all elements was not refined. To achieve the electroneutrality for $LaNi_{0.5}Ti_{0.45}Co_{0.05}O_3$ perovskite, the fraction of site occupancy for *B*-cations was divided and fixed into four parts: 0.225 for Ni^{2+} or Ti^{4+} and 0.025 for Ni^{3+} or Co^{3+}. For $LaNi_{0.45}Co_{0.05}Ti_{0.5}O_3$ perovskite, this value was divided and fixed into three parts: 0.25, 0.225, and 0.025 for Ti^{4+}, Ni^{2+}, and Co^{2+}, respectively. For $LaNi_{0.5}Ti_{0.5}O_3$ perovskite, the fraction of site occupancy for *B*-cations was equal and fixed to 0.25 for Ti^{4+} and Ni^{2+} (ICSD, 2017).

III. RESULTS AND DISCUSSION

Chemical composition (weight percentage basis) obtained from X-ray fluorescence, unit-cell parameters, X-ray densities, atomic coordinates, *B*-cation to metal bond distances, and agreement factors from Rietveld refinement of powder XRD data for as-synthesized materials are indicated in Table I.

The chemical composition was close to their corresponding nominal values, whose variation was attributed to experimental error. Therefore, it supports the expected composition. Experimental, calculated, and difference XRD patterns are shown in Figure 1. Impurity phases were not detected in XRD patterns of the as-synthesized materials. The unit-cell parameters for as-synthesized materials are similar to the respective for $LaNi_{0.5}Ti_{0.5}O_3$ (ICSD, 2017). X-ray density for $LaNi_{0.5}Ti_{0.5}O_3$ perovskite is similar to the reported literature value (6.643 vs. 6.631 g cm^{-3}; Table I). For $LaNi_{0.5}Ti_{0.45}Co_{0.05}O_3$ (6.685 vs. 6.631 g cm^{-3}; Table I) and $LaNi_{0.45}Co_{0.05}Ti_{0.5}O_3$ (6.661 vs. 6.631 g cm^{-3}; Table I), the variations of X-ray density are expected due to chemical composition. Metal-to-oxygen bond distances and bonding angles are close to values reported in the literature, except the *B*–O1 and *B*–O2 bond distances for the perovskite obtained from the partial substitution of Ti^{4+} by Co^{2+} in 0.05 mol. These results are attributed to different values of metal-to-oxygen bond distances for *B*-cations with two different valences (Ni^{2+}, Ni^{3+}, Ti^{4+}, and Co^{3+}) assumed for the achievement of electroneutrality. Since *R* factors from Rietveld refinement can be improved by increasing the counting time per step and decreasing the step size of powder XRD data acquisition, agreement factors were acceptable for the used experimental conditions. It is worth mentioning that we reported magnetic measurements for $LaNi_{0.5}Ti_{0.5}O_3$ perovskite and temperature-programmed reduction for the as-prepared materials in a previous work (Tuza and Souza, 2017). Magnetic measurements support the assumed symmetry for $LaNi_{0.5}Ti_{0.5}O_3$ perovskite. Also, $LaNi_{0.5}Ti_{0.45}Co_{0.05}O_3$ is difficult to reduce, when compared with the other as-synthesized perovskites, which can be attributed to some nickel and all the cobalt with a valence equal to 3+. Therefore, the symmetry of as-prepared perovskites is orthorhombic, with space group *Pbnm,* and glazer notation $a^-a^-c^+$ (Martin and Parise, 2008; Fowlie, 2019). The powder diffraction data of as-synthesized perovskites are provided in Tables II–IV. The indexation of the powder XRD pattern from each sample was carried out using the

https://doi.org/10.1017/S0885715620000767 Published online by Cambridge University Press

TABLE III. Powder diffraction data of $LaNi_{0.45}Co_{0.05}Ti_{0.5}O_3$.

$2\theta_{obs}$ (°)[a]	d_{obs} (Å)	$(I/I_0)_{obs}$	h	k	l	$2\theta_{calc}$ (°)[b]	$2\theta_{calc}$ (°)[c]	d_{calc} (Å)[d]	$\Delta 2\theta$ (°)[e]
22.744	3.907	99.5	0	0	2	22.739	22.710	3.912	0.006
32.374	2.763	1000	1	1	2	32.370	32.334	2.766	0.004
39.912	2.257	155.4	2	0	2	39.909	39.853	2.260	0.003
46.448	1.953	327.4	2	2	0	46.440	46.379	1.956	0.008
47.930	1.896	13.9	2	2	1	47.922	47.894	1.898	0.008
52.292	1.748	42.8	2	2	2	52.303	52.239	1.750	−0.011
57.715	1.596	190.9	3	1	2	57.701	57.630	1.598	0.014
58.937	1.566	3.5	2	2	3	58.978	58.972	1.565	−0.041
67.720	1.382	170.1	2	2	4	67.732	67.680	1.383	−0.012
72.407	1.304	18.9	3	1	4	72.415	72.374	1.305	−0.008
73.664	1.285	7.3	3	3	1	73.673	73.568	1.286	−0.010
74.760	1.269	1.2	1	4	2	74.737	74.784	1.268	0.023
77.038	1.237	72.9	3	3	2	77.032	77.013	1.237	0.006
86.093	1.128	44.7	4	0	4	86.086	85.942	1.130	0.007
87.131	1.118	11.2	2	4	3	87.128	87.165	1.117	0.003

F(20) = 19.87 (0.0082, 123) (Smith and Snyder, 1979).
[a]Corrected observed peak positions.
[b]Peak positions calculated using the McMaille program.
[c]Peak positions calculated using the Fullprof program.
[d]Interplanar distance calculated using the Fullprof program.
[e]$\Delta 2\theta$ (°) = $^a2\theta_{obs}$ (°) − $^b2\theta_{calc}$ (°).

TABLE IV. Powder diffraction data of $LaNi_{0.5}Ti_{0.5}O_3$.

$2\theta_{obs}$ (°)[a]	d_{obs} (Å)	$(I/I_0)_{obs}$	h	k	l	$2\theta_{calc}$ (°)[b]	$2\theta_{calc}$ (°)[c]	d_{calc} (Å)[d]	$\Delta 2\theta$ (°)[e]
22.713	3.912	98.8	0	0	2	22.713	22.683	3.917	−0.001
32.315	2.768	1000	1	1	2	32.315	32.303	2.769	0.001
39.868	2.259	148.7	2	0	2	39.864	39.824	2.262	0.004
41.585	2.170	6.7	1	1	3	41.561	41.535	2.172	0.025
43.118	2.096	4	1	2	2	43.149	43.2	2.092	−0.031
46.382	1.956	323.2	2	2	0	46.386	46.343	1.958	−0.004
52.221	1.750	42.5	2	2	2	52.227	52.194	1.751	−0.006
57.661	1.597	191.6	3	1	2	57.661	57.591	1.599	−0.001
63.919	1.455	1.6	3	1	3	63.900	63.942	1.455	0.019
67.639	1.384	152.8	2	2	4	67.636	67.608	1.385	0.003
72.244	1.307	17.3	3	1	4	72.261	72.307	1.306	−0.017
72.417	1.304	7.7	0	4	2	72.419	72.389	1.304	−0.003
78.071	1.223	4.7	2	2	5	78.056	78.059	1.223	0.015
81.334	1.182	10.5	2	0	6	81.318	81.418	1.181	0.016
81.440	1.181	26.5	4	2	2	81.443	81.427	1.181	−0.004
82.501	1.168	0.9	3	1	5	82.519	82.537	1.168	−0.018
85.971	1.130	41.6	4	0	4	85.969	85.868	1.131	0.002
89.180	1.097	0.1	5	0	1	89.183	89.187	1.097	−0.003

F(20) = 17.50 (0.0085, 134) (Smith and Snyder, 1979)
[a]Corrected observed peak positions.
[b]Peak positions calculated using the McMaille program.
[c]Peak positions calculated using the Fullprof program.
[d]Interplanar distance calculated using the Fullprof program.
[e]$\Delta 2\theta$ (°) = $^a2\theta_{obs}$ (°) − $^b2\theta_{calc}$ (°).

McMaille program (Le Bail, 2004). Moreover, the crystal structure of the as-prepared samples is indicated in Figure 1, which was drawn using VESTA software (Momma and Izumi, 2011).

A representative FEG-SEM image of $LaNi_{0.5}Ti_{0.5}O_3$ is shown in Supplementary Figure S1. Related to this perovskite, grains are composing elongated and spherical particles at the range 15.5–128.1 nm, with mean particle size equal to 57.3 nm. Grain population with particle size less than 100 nm was equal to 87.3%. This result is in accordance with the average crystallite size determined by the Scherrer equation (27.1 nm; Table I). It is worth noting that the average crystallite size for $LaNi_{0.5}Ti_{0.45}Co_{0.05}O_3$ (35.8 nm; Table I) and $LaNi_{0.45}Co_{0.05}Ti_{0.5}O_3$ (32.7 nm; Table I) was similar to the corresponding for $LaNi_{0.5}Ti_{0.5}O_3$. As the synthesis method was the same for all the perovskites, i.e., the same calcination temperature was employed to synthesize all the perovskites, we concluded that $LaNi_{0.5}Ti_{0.45}Co_{0.05}O_3$, $LaNi_{0.45}Co_{0.05}Ti_{0.5}O_3$, and $LaNi_{0.5}Ti_{0.5}O_3$ materials are composed mainly by nanoparticles.

https://doi.org/10.1017/S0885715620000767 Published online by Cambridge University Press

IV. CONCLUSIONS

$LaNi_{0.5}Ti_{0.45}Co_{0.05}O_3$, $LaNi_{0.45}Co_{0.05}Ti_{0.5}O_3$, and $LaNi_{0.5}Ti_{0.5}O_3$ perovskites were synthesized by the modified Pechini method. The chemical composition of these materials was close to nominal values, which indicated the appropriate application of the synthesis method. The as-prepared perovskites are composed largely by nanoparticles, with orthorhombic crystal structure, space group *Pbnm,* and glazer notation $a^-a^-c^+$. XRD data affirmed the single-phase of each as-prepared material.

V. DEPOSITED DATA

CIF files with information related to as-prepared perovskites, RAW, and DAT files with XRD data of these materials were deposited with the ICDD. You may request this data from ICDD at info@icdd.com.

SUPPLEMENTARY MATERIAL

The supplementary material for this article can be found at https://doi.org/10.1017/S0885715620000767.

ACKNOWLEDGEMENTS

The authors thank Carlos André de Castro Perez from Instituto Federal de Ciência e Tecnologia do Rio de Janeiro – IFRJ, Brazil, for Rietveld analysis suggestions. Also, they are grateful to Andréa Maria Duarte de Farias and Francisco Luiz Correa Rangel from Nanotechnology Characterization Center (CENANO)/National Institute of Technology, Brazil for SEM images used to determine the particle size of as-synthesized perovskites.

CONFLICTS OF INTEREST

The authors have no conflicts of interest to declare.

Anderson, M. T., Greenwood, K. B., Taylor, G. A., and Poeppelmeier, K. R. (**1993**). "B-cation arrangements in double perovskites," Prog. Solid State Chem. **22**(3), 197–233.

Attfield, M., Barnes, P., Cockcroft, J. K., and Driessen, H. (**2004**). *Advanced Certificate in Powder Diffraction* (School of Crystallography, Birkbeck College, University of London). Available at: http://pd.chem.ucl.ac.uk/pdnn/chapter.htm.

Campbell, K. D. (**1992**). "Layered and double perovskites as methane coupling catalysts," Catal. Today **13**(2–3), 245–253.

Deng, Z. Q., Smit, J. P., Niu, H. J., Evans, G., Li, M. R., Xu, Z. L., Claridge, J. B., and Rosseinsky, M. J. (**2009**). "B cation ordered double perovskite $Ba_2CoMo_{0.5}Nb_{0.5}O_{6-\delta}$ as a potential SOFC cathode," Chem. Mater. **21** (21), 5154–5162.

Ezzahi, A., Manoun, B., Ider, A., Bih, L., Benmokhtar, S., Azrour, M., Azdouz, M., Igartua, J. M., and Lazor, P. (**2011**). "X-ray diffraction and Raman spectroscopy studies of $BaSrMWO_6$ (M=Ni, Co, Mg) double perovskite oxides," J. Mol. Struct. **985**(2–3), 339–345.

Fowlie, J. (**2019**). *Electronic and Structural Properties of $LaNiO_3$-Based Heterostructures* (Springer, Cham), p. 2.

Hayakawa, T., Harihara, H., Andersen, A. G., Suzuki, K., Yasuda, H., Tsunoda, T., Hamakawa, S., York, A. P. E., Yoon, Y. S., Shimizu, M., and Takehira, K. (**1997**). "Sustainable $Ni/Ca_{1-x}Sr_xTiO_3$ catalyst prepared *in situ* for the partial oxidation of methane to synthesis gas," Appl. Catal., A **149**(2), 391–410.

Huang, Y. H., Liang, G., Croft, M., Lehtimäki, M., Karppinen, M., and Goodenough, J. B. (**2009**). "Double-perovskite anode materials Sr_2MMoO_6 (M=Co, Ni) for solid oxide fuel cells," Chem. Mater. **21** (11), 2319–2326.

ICSD (**2017**). Inorganic Crystal Structure Database (Database), 76344 Eggenstein-Leopoldshafen, Germany.

Iulianelli, A., Liguori, S., Wilcox, J., and Basile, A. (**2016**). "Advances on methane steam reforming to produce hydrogen through membrane reactors technology: a review," Catal. Rev. **58**(1), 1–35.

Le Bail, A. (**2004**). "Monte Carlo indexing with McMaille," Powd. Diffr. **19** (3), 249–254.

Li, C., Wang, W., Zhao, N., Liu, Y., He, B., Hu, F., and Chen, C. (**2011**). "Structure properties and catalytic performance in methane combustion of double perovskites $Sr_2Mg_{1-x}Mn_xMoO_{6-\delta}$," Appl. Catal., B **102**(1–2), 78–84.

Martin, C. D. and Parise, J. B. (**2008**). "Structure constraints and instability leading to the post-perovskite phase transition of $MgSiO_3$," Earth Planet. Sci. Lett. **265**(3–4), 630–640.

Mefford, J. T., Hardin, W. G., Dai, S., Johnston, K. P., and Stevenson, K. J. (**2014**). "Anion charge storage through oxygen intercalation in $LaMnO_3$ perovskite pseudocapacitor electrodes," Nat. Mater. **13**(7), 726–732.

Momma, K. and Izumi, F. (**2011**). "VESTA 3 for three-dimensional visualization of crystal, volumetric and morphology data," J. Appl. Crystallogr. **44**, 1272–1276.

Pérez-Flores, J. C., Ritter, C., Pérez-Coll, D., Mather, G. C., García-Alvarado, F., and Amador, U. (**2011**). "Synthesis, structures and electrical transport properties of the $La_{2-x}Sr_xNiTiO_{6-\delta}$ $(0 \le x \le 0.5)$ perovskite series," J. Mater. Chem. **21**(35), 13195–13204.

Provendier, H., Petit, C., and Kiennemann, A. (**2001**). "Steam reforming of methane on $LaNi_xFexO_3$ (0<=*x*<=1) perovskites. Reactivity and characterisation after test," C. R. Acad. Sci., Ser. IIc: Chim., **4**(1), 57–66.

Rodríguez, E., Álvarez, I., López, M. L., Veiga, M. L., and Pico, C. (**1999**). "Structural, electronic, and magnetic characterization of the perovskite $LaNi_{1-x}Ti_xO_3$ $(0 \le x \le 12)$," J. Solid State Chem. **148**(2), 479–486.

Rodríguez, E., López, M. L., Campo, J., Veiga, M. L., and Pico, C. (**2002**). "Crystal and magnetic structure of the perovskites La_2MTiO_6 (M = Co, Ni)," J. Mater. Chem. **12**(9), 2798–2802.

Rodríguez-Carvajal, J. (**1993**). "Recent advances in magnetic structure determination by neutron powder diffraction," Physica B. **192**(1–2), 55–69.

Rodríguez-Carvajal, J. (**2001**). Fullprof Manual (Report). Grenoble: Institute Laue Langevin.

Shaheen, R. and Bashir, J. (**2010**). "Ca_2CoNbO_6: a new monoclinically distorted double perovskite," Solid State Sci. **12**(8), 1496–1499.

Smith, G. S. and Snyder, R. L. (**1979**). "FN: a criterion for rating powder diffraction patterns and evaluating the reliability of powder-pattern indexing," J. Appl. Crystallogr. **12**, 60–65.

Tuza, P. V. and Souza, M. M. V. M. (**2016**). "Steam reforming of methane over catalyst derived from ordered double perovskite: effect of crystalline phase transformation," Catal. Lett. **146**(1), 47–53.

Tuza, P. V. and Souza, M. M. V. M. (**2017**). "B-cation partial substitution of double perovskite La_2NiTiO_6 by Co^{2+}: effect on crystal structure, reduction behavior and catalytic activity," Catal. Commun. **97**(1), 93–97.

Urasaki, K., Sekine, Y., Kawabe, S., Kikuchi, E., and Matsukata, M. (**2005**). "Catalytic activities and coking resistance of Ni/perovskites in steam reforming of methane," Appl. Catal., A **286**(1), 23–29.

Yang, W. Z., Liu, X. Q., Lin, Y. Q., and Chen, X. M. (**2012**). "Structure, magnetic, and dielectric properties of $La_2Ni(Mn_{1-x}Ti_x)O_6$ ceramics," J. Appl. Phys. **111**, 084106.

Zohuri, B. (**2019**). *Small Modular Reactors as Renewable Energy Sources* (Springer, Gewerbestrasse), p. 198.